Journal of Solid State Chemistry 182 (2009) 2141–2148

Contents lists available at ScienceDirect

Journal of Solid State Chemistry

journal homepage: www.elsevier.com/locate/jssc

Hierarchical control of porous silica by pH adjustment: Alkyl polyamines as surfactants for bimodal silica synthesis and its carbon replica

G. Abellán, A.I. Carrillo, N. Linares, E. Serrano, J. García-Martínez *

Molecular Nanotechnology Lab, Universidad de Alicante, Ctra. Alicante—San Vicente s/n, E-03690, Alicante, Spain

ARTICLE INFO

Article history:
Received 5 February 2009
Received in revised form
20 April 2009
Accepted 27 May 2009
Available online 2 June 2009

Keywords:
Bimodal mesopore materials
Templated mesopores
Surfactant
Carbon replica
Silica

ABSTRACT

Bimodal macro-mesoporous silica networks have been prepared in a simple one-pot synthesis using an inexpensive tetramine surfactant and tetraethoxysilane as a silica precursor. These novel materials show high pore volumes and templated mesopores (average pore size 3.0 nm) embedded in 20 nm thick walls forming interparticle large meso/macropores. The judicious control of the pH during the silica formation allows for the precise control of the interparticle condensation, likely due to the change in the interaction between the tetramine surfactant and the silica precursors. Finally, a highly porous carbon replica with bimodal porosity was prepared by using the bimodal silica as a hard sacrificial template. The microstructure of the silica template was accurately transferred to the carbon material obtaining high surface areas (up to 1300 $m^2 g^{-1}$) and total pore volumes $\geq 2\,cm^3 g^{-1}$.

1. Introduction

Mesostructured solids have attracted much attention in the last years due to their wide range of applications in catalysis, controlled drug-delivery, separation techniques, optical devices and sensors [1–6]. Surfactant-templated synthesis is a convenient and widely used technique for the preparation of mesostructured materials [2,3] with some remarkable properties, such as high surface area and narrow pore size distribution [4–8]. Multimodal materials combine the benefits of high surface area due to their micro- and/or mesoporosity with enhanced accessibility thanks to an open structure [1,9], which has been proved to remarkably improve their accessibility and therefore their catalytic activity for large molecules [10,11].

The synthesis of materials with various pore combinations such as micro-mesopores, micro-macropores, meso-macropores, or even trimodal micro-meso-macropores, has been carried out using various smart strategies [12,13]. For example, Wang et al. [14,15] reported the synthesis of bimodal mesoporous silica using ammonia as catalyst at room temperature and cetyltrimethylammonium bromide (CTAB) as a surfactant. By adjusting the pH and the ammonia/silica molar ratio a hierarchical porous silica xerogel was easily obtained. Zhang et al. [16] have described the synthesis of bimodal nanoparticulated silica using a single non-ionic templating surfactant. Also, the use of silica precursors that allows to control the kinetics of the nucleation and growth process, have been described to prepare small silica nanoparticles that form large interparticle pores [7,17–36]. Recently, Muto et al. [37] reported the effect of pH on the mesostructures of silica materials obtained from cationic surfactants (CTA^+Cl^-) and silicic acid prepared by the ion exchange of sodium silicate solution. It is also possible to combine the use of a soft template (typically a surfactant) with a hard template, like S. Mann and co-workers did to prepare macroporous sponge-like monoliths and mesoporous thin films using starch gels and sponges in combination with preformed silicalite nanoparticles [12].

Using a modified synthesis of the so called ''atrane route'', P. Amorós and co-workers [7,9,17] have synthesized a novel bimodal mesoporous material with pore volumes in excess of $2.0\,cm^3 g^{-1}$. The strategy is based on the use of complexes like atranes or silatranes as hydrolytic inorganic precursors and cationic surfactants as templates. Using this strategy, SBA-15 or MCM-41 type mesoporous materials have been successfully prepared in a one-pot surfactant-assisted procedure by using these surfactants [17]. It has been shown that both the pore and particle sizes in hierarchical porous silica are highly dependent on the surfactant nature [7,9]. Based on this learning, we have used a novel surfactant (a commercially available inexpensive polyamine) that favours the formation of small silica particles, and therefore the creation of large interparticle porosity by judicious control of the pH to favour the interaction of the positively charged surfactant and the negatively charged silica precursors.

* Corresponding author. Fax: +34 965903454.
E-mail address: j.garcia@ua.es (J. García-Martínez).
URL: http://www.nanomol.es (J. García-Martínez).

0022-4596/$ - see front matter © 2009 Elsevier Inc. All rights reserved.
doi:10.1016/j.jssc.2009.05.033

On the other hand, porous carbon materials with high surface areas and pore volumes are of interest for energy storage, separation, catalysis, and other applications [13,38,39]. The use of porous silica materials as templates is widely employed to synthesize carbon replicas with both porous [40–43] and hierarchical structures [44–49]. In general, the silica template is impregnated with a carbon precursor (typically furfuryl alcohol, phenol resin or sucrose) followed by the curing and carbonization of the organic/inorganic composite. Finally, the silica template is removed by chemical treatment in a HF or NaOH solution [40,41,44,46,50,51]. Recently Pérez-Cabrero and co-workers reported the synthesis of a mesoporous carbon with 720 $m^2 g^{-1}$ and a bimodal pore system using acetylene CVD to replicate a bimodal silica, obtaining an accurate carbon replica with semi-crystalline porous walls. The authors suggested potential applications in catalysis [52].

Herein we describe the one-pot synthesis of a bimodal porous silica network (BSN) prepared at room temperature in the presence of a low cost surfactant (tallow tetramine) by systematically varying pH conditions. The pH control allows for systematically tuning the interparticle porosity and, therefore easily preparing a bimodal silica network with high pore volume and high BET area. In a second step, the as-synthesized BSN have been used as hard template for the preparation of bimodal carbon replicas using sucrose and sulphuric acid as the carbon source and catalyst, respectively.

2. Experimental

2.1. Materials

The surfactant used as template for the synthesis of silica materials was a polyamine, trade named tallow tetramine, kindly supplied by Tomah3 Products Inc. According to the supplier, the molecular formula of tallow tetramine is R–$[NH(CH_2)_3]_3NH_2$, being R mostly C18 with some C16 and some insaturations. All reagents, tallow tetramine, tetraethylorthosilicate (98%, Aldrich, denoted as TEOS), ammonium hydroxide (30%, Sigma-Aldrich, NH_4OH), hydrochloric acid (37%, Fluka, HCl), acetic acid (98.5%, Panreac, CH_3COOH), sulphuric acid (96%, Sigma-Aldrich, H_2SO_4), sucrose (Aldrich, $C_{12}H_{22}O_{11}$) and fluorhydric acid (48%, Aldrich, HF) were used as received without further purification.

2.2. Synthesis of bimodal mesoporous silica materials (BSN)

In a typical synthesis, 7.15 g of surfactant (tallow tetramine, 1.6 10^{-2} mol) was magnetically stirred (600 rpm) in 650 ml of deionised water at room temperature, in a closed flask, until a clear solution was obtained (approximately 24 h) being the pH = 11. Following, the hydrolysis of 35.4 g of TEOS (1.7×10^{-1} mol, n(surfactant):n(TEOS) molar ratio = 0.1:1) was carried out by base or non-catalyzed hydrolysis in the presence of tallow tetramine. After 15 h of orbital stirring at room temperature, a white suspension was obtained. It should be noted that, for non-catalyzed hydrolysis, the pH falls down from 11.0 to 9.4, as expected due to silica condensation reactions. To study the effect of the pH on the porosity properties of the final material, the pH was slowly adjusted in 8–11 range using either aqueous NH_4OH (30%) or HCl (10%) and compared with that obtained without the addition of any pH controlling agent (pH final = 9.4). The so obtained solids were washed first with water and then with ethanol, filtered out, and air dried. Finally, the surfactant was removed by calcination at 550 °C for 8 h (10 °C min^{-1}) under static air atmosphere. The key properties of the samples synthesized by systematically varying the hydrolysis conditions, i.e. pH of the final solutions, are summarized in Table 1. In order to study the role of the surfactant in the formation of mesoporosity, additional experiments with ten-fold lower surfactant/TEOS molar, i.e., n(surfactant):n(TEOS) = 0.01:1 were carried. Furthermore, the same synthesis conditions were tested in open flasks. The main properties of a representative bimodal silica sample are shown in Table 2.

2.3. Synthesis of bimodal mesoporous carbon materials

The synthesis of the mesoporous carbons was performed using sucrose as carbon source and sulphuric acid as polymerization catalyst to accelerate the carbonization of sucrose, similar to the method used by Ryoo et al. [40]. The calcined mesostructured silica (BSN) was firstly impregnated with a solution of sucrose (typically 1.25 g of sucrose per gram of silica, 3.6×10^{-3} mol) in aqueous sulphuric acid solution (0.28 mol L^{-1}), and afterwards thermally treated in air for 6 h at 100 °C and 6 h at 200 °C to partially polymerize the sucrose, the sample turned black during this pre-treatment. Subsequently, a second solution containing 0.8 g sucrose (2.0×10^{-4} mol) in sulphuric acid solution (0.2 mol L^{-1}) was added to this material. The impregnated sample was cured in air for 6 h at 100 °C and 6 h at 200 °C to polymerize the sucrose [41,43,53], which was then carbonized in a tubular oven under N_2 atmosphere at 900 °C (2 °C min^{-1}). The molar composition of the synthesis mixture was as follows: n(H_2O):n(H_2SO_4):n(SiO_2):n(sucrose) = 57.5:0.22:1:0.55.

The resulting carbon–silica composite was stirred overnight in 15% HF at room temperature to remove the silica template. The material obtained as an insoluble fraction was washed with distilled water and then dried in air at room temperature.

Table 1
Textural parameters of different bimodal macro-mesoporous silica networks obtained by systematically varying the hydrolysis conditions.

Sample	pH[a]	Surface area ($m^2 g^{-1}$)[b]	Mesopore volume ($cm^3 g^{-1}$)[c]	Interparticle volume ($cm^3 g^{-1}$)[c]	Total pore volume ($cm^3 g^{-1}$)[c]	Mesopore size (nm)[d]	Large mesopore size (nm)[d]
BSN1	8	790–810	0.6	0.4	1.0	3.0	10–13
BSN2	9.4	710–800	0.6	0.9	1.5	3.0	25–30
BSN3	10	840–890	0.55–0.65	1.45–1.55	2.0–2.1	2.5–3.0	(*)
BSN4	11	730–940	0.5–0.6	0.9–1.5	1.5–1.9	2.7–3.0	(*)

(*) Out of range of nitrogen adsorption technique.

[a] pH of final solutions.

[b] The BET surface area was estimated by using multipoint BET method using the adsorption data in the relative pressure (P/P_0) range of 0.05–0.30.

[c] Mesopore volume was calculated from the adsorption branch of the nitrogen isotherm using the BJH method, the volume was measured at the plateau of the cumulative adsorption pore volume plot (approximately 8 nm). The total pore volume was measured at $P/P_0 = 0.99$. The pore volume of the large mesopore, interparticle, volume, was estimated subtracting both values.

[d] Average mesopore and large mesopore sizes were estimated from the adsorption branch of the nitrogen isotherm using the BJH method.

Table 2
Textural parameters of mesoporous carbons (sucrose/silica molar ratio = 0.55) as compared with their BSN precursors (pH = 9.5–10).

Sample	Surface area ($m^2 g^{-1}$)[a]	Mesopore volume ($cm^3 g^{-1}$)[b]	Total pore volume ($cm^3 g^{-1}$)[b]	Mesopore size (nm)[c]	Large mesopore size (nm)[c]	Carbon content (%)[d]
BSN5	685–702	0.60	1.4–1.7	3.5	35–42	–;
Carbon	1190–1300	0.90	≥2.0	3.5	30–42	25–38

[a] The BET surface area was estimated by using multipoint BET method using the adsorption data in the relative pressure (P/P_0) range of 0.05–0.30.
[b] Mesopore volume was calculated from the adsorption branch of the nitrogen isotherm using the BJH method, the volume was measured at the plateau of the cumulative adsorption pore volume plot (approximately 8 nm). The total pore volume was measured at $P/P_0 = 0.99$. The pore volume of the large mesopore, interparticle, volume, was estimated subtracting both values.
[c] Average mesopore and large mesopore sizes were estimated from the adsorption branch of the nitrogen isotherm using the BJH method.
[d] Carbon fraction in carbon–silica composite before silica template removal estimated by weight differences before and after HF treatment, washing and drying in air atmosphere.

2.4. Characterization

The porous texture of all the materials prepared was characterized by N_2 adsorption at 77 K in an AUTOSORB-6 apparatus. The samples were previously degassed for 4 h at 523 K at 5×10^{-5} bar. The adsorption branch was used to determine the pore size distribution and mesopores volume using the Barret–Joyner–Helender (BJH) method. The mesoporous volume was measured at the plateau of the cumulative adsorption pore volume plot (approximately 8 nm). The total pore volume was measured at $P/P_0 = 0.99$. The pore volume of the large mesopore, interparticle, volume, was estimated subtracting both values. The surface area was determined using the BET method in the 0.05 to 0.30 relative pressure range.

The morphology of the mesoporous materials was investigated by transmission electron microscopy (TEM) and scanning electron microscopy (SEM). TEM studies were carried out on a JEM-2010 microscope (JEOL, Japan). The instrument, operated at 200 kV, has a resolution of 0.14 nm. Samples for TEM studies were prepared by dipping a sonicated suspension of the sample in ethanol on a carbon-coated copper grid. The digital analysis of the TEM micrographs was done using DigitalMicrographTM 3.6.1. by Gatan. SEM analysis of all the samples, previously covered with gold, was carried out using a JSM-840 microscope (JEOL, Japan).

Small-angle powder X-ray diffraction (XRD) analysis was carried out with a Bruker Axs D5005 powder X-ray diffractometer using Cu$K\alpha$ radiation ($\lambda = 1.54056$ Å) at 40 kV and 30 mA.

Thermogravimetric analysis (TGA) was performed on the Mettler Toledo TG/SDTA analyzer. The measurement was carried out under nitrogen atmosphere from room temperature to 1100 °C, with a heating rate of 10 °C min^{-1}.

3. Results and discussion

3.1. Characterization of bimodal silica networks

Table 1 contains some relevant textural parameters of BSN materials for each of the synthesis conditions described in the previous section. It should be noted that each experiment has been performed several times in order to evaluate the reproducibility of our synthesis method, and it is for that reason that all the property values shown in this article range within the results obtained for each sample. Representative nitrogen adsorption/desorption isotherms for each synthesis conditions and their corresponding pore size distributions are shown in Fig. 1(a) and (b), respectively. For comparison purposes, the adsorption branch of the nitrogen isotherm corresponding to a silica material synthesized using a ten-fold lower surfactant/TEOS molar ratio, i.e., n(surfactant):n(TEOS) = 0.01:1, at pH = 10.5 is included in Fig. 1a. BSN materials show type IV isotherms with two distinctive

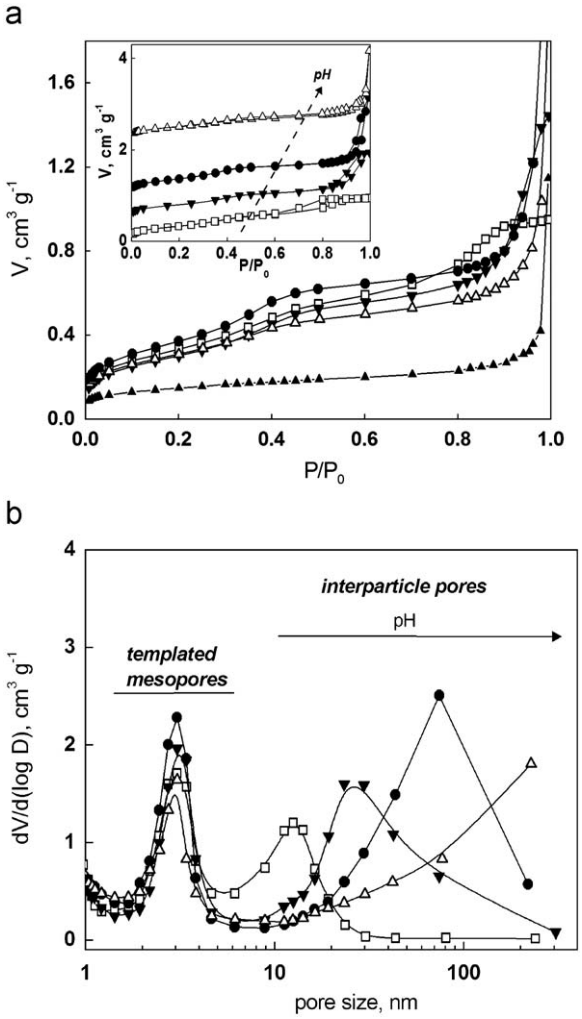

Fig. 1. (a) Adsorption branch of nitrogen isotherms at 77 K for: (–□–) BSN1, pH = 8, (–▼–) BSN2, pH = 9.4, (–●–) BSN3, pH = 10, (–△–) BSN4, pH = 11 and (–▲–) the silica material synthesized by diminishing the surfactant/TEOS molar ratio 10 times, i.e., n(surfactant):n(TEOS) = 0.01:1. The inset show full nitrogen adsorption/desorption isotherms for BSN materials, where isotherms for BSN samples at pH 9.4, 10 and 11 are shifted 0.4, 1.0 and 2.2 $cm^3 g^{-1}$, respectively, for clarity. (b) Pore size distributions of BSN1–4 materials calculated from the adsorption branch using the BJH method. The corresponding textural parameters are shown in Table 1.

nitrogen uptakes at $P/P_0 = 0.3$ and 0.8–0.9 thus indicating the presence of a bimodal porosity (Fig. 1(a)). The first adsorption uptake appears at a relative pressures close to $P/P_0 = 0.3$ independently of the pH conditions used to prepare the sample. This feature is related to capillary nitrogen condensation in the

intraparticle mesopores [7]. The size of these mesopores (around 3 nm in diameter), shown in the pore size distribution plot (Fig. 1(b)), are typical of surfactant-templated silica materials. Their size and relative volume ($0.6\,cm^3\,g^{-1}$) are similar for all the samples prepared indicating that the formation of surfactant-templated mesopores is not affected by the pH conditions in the 8–11 range. When the n(surfactant):n(TEOS) molar ratio was ten-fold decreased with respect to that used for BSN1-5 samples (from n(surfactant):n(TEOS) = 0.1:1 to 0.01:1), the nitrogen isotherm of these materials shows only one gas uptake at relative pressures near to 1.0, being the BET are of around $320\,m^2/g$ (see Fig. 1(a)). This observation suggests that the intraparticle mesopores are due to the surfactant templating effect.

Following with the pH effect on BSN materials, as can be seen in Fig. 1(a), the second gas uptake, which is due to the filling of much larger mesopores or even macropores, occurs at higher relative pressures ($P/P_0 > 0.8$) and it moves toward higher relative pressures as pH increases. Accordingly, the interparticle pore size and, consequently, the interparticle pore volume and the total pore volume also increase as pH does (Fig. 1(b)). In all cases, only the second uptake shows a hysteresis loop, indicating an irregularly shaped interparticle porosity. In addition, no significant differences can be observed in the BET areas (see Table 1). This observation is consistent with the similarity of all the isotherms in the P/P_0 range used to calculate the BET surface areas. Furthermore, these results indicate that nitrogen condensation inside the templated mesopores have a higher contribution to the BET surface area than the large mesopores/macropores, since the increase of the interparticle pore volumes as pH increases has a little effect on the BET surface area of these materials.

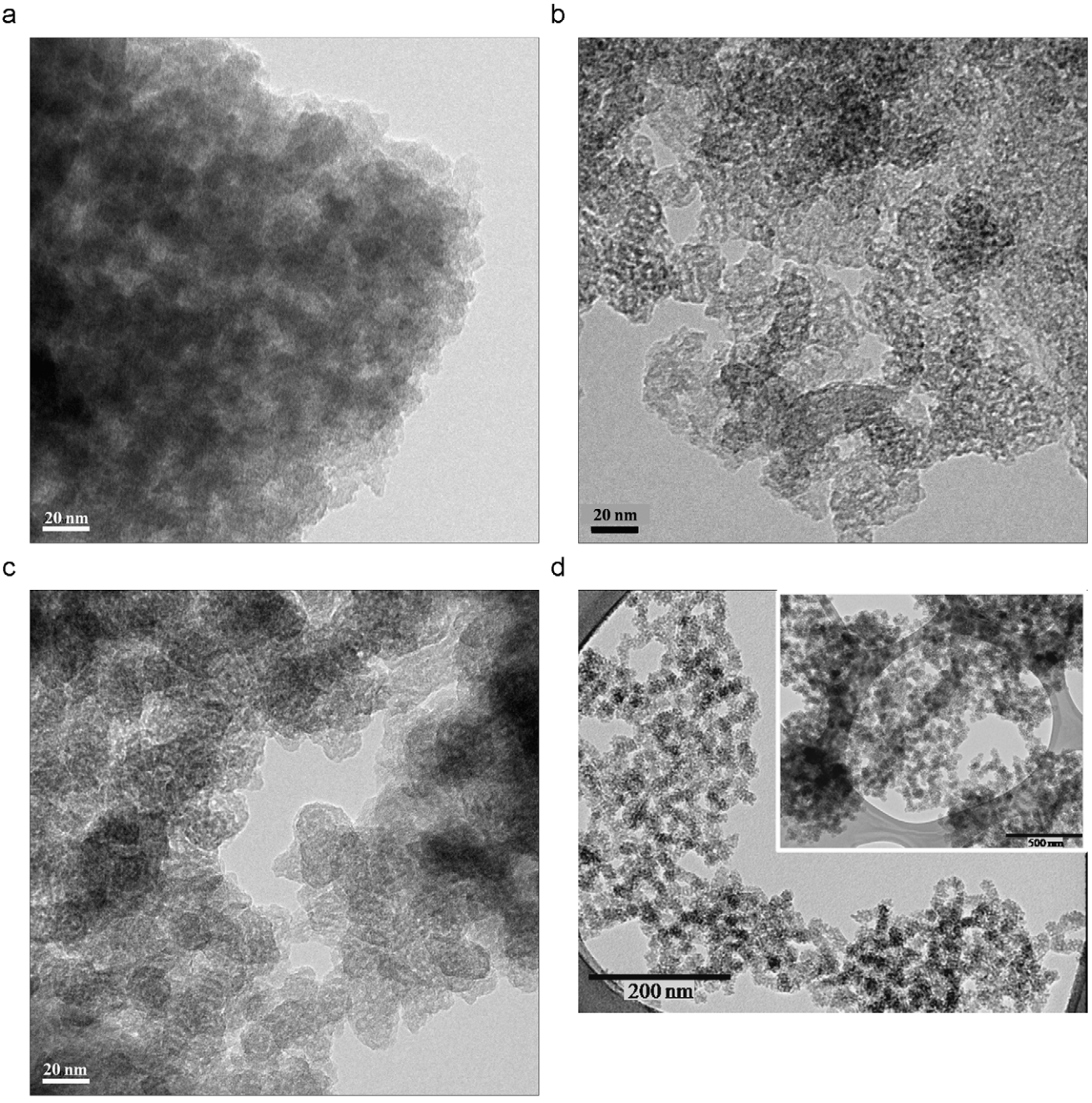

Fig. 2. Representative TEM images of calcined BSN materials: (a) BSN1, pH = 8, (b) BSN2, pH = 9.4, (c) BSN3, pH = 10 and (d) BSN3 sample under magnetic conditions at lower magnification. The inset in (d) shows the same material even at lower magnification.

For BSN synthesized upon HCl addition (BSN1, pH = 8), mesopores of ca. 10 nm with low interparticle volume and, consequently, low total pore volume are obtained (Table 1). The corresponding TEM image (Fig. 2(a)) confirms the formation of a poor bimodal porous network. When BSN were synthesized without the addition of neither ammonia nor HCl (sample BSN2 in Table 1) an increase in the interparticle volume and, consequently, the total pore volume is observed. In this case, the interparticle pore size increase up to 25–30 nm and, as shown in Fig. 2(b), TEM analysis confirms an open bimodal network in which both small mesopores and large mesopores can be observed. The addition of ammonia to increase the pH of the final solutions up to 10–11 leads to even higher total pore volume. The pore size distribution plot (Fig. 1(b)) shows a shift of the second peak (corresponding to interparticle pores) as pH increases. For those samples prepared at higher pH (BSN3 and BSN4) the pore size determination was not possible. As example, a representative TEM micrograph for BSN at pH = 10 (sample BSN3 in Table 1) is shown in Fig. 2(c). Besides the bimodal character of these materials, the morphology of BSN3 indicates a very open structure. Fig. 2(d) shows, at lower magnification, the bimodal structure of sample BSN3 prepared under magnetic stirring. Both the intraparticle and interparticle porosity can be clearly distinguished. Noteworthy, the intraparticle mesoporosity is no ordered and the particles show a very rough surface.

On the other hand, the same synthesis has been carried out in open flask and compared with those corresponding to the closed flask synthesis. The key properties of the so prepared BSN materials synthesized at pH in 9.5–10 range (BSN5) are shown in Table 2. Its corresponding nitrogen isotherm and pore size distribution are presented in Fig. 3(a) and (b), respectively, and a representative TEM micrograph for this material is shown in Fig. 4bI. There are no significant differences with its analogues synthesized in closed flask, i.e. BSN2 and BSN3. As observed for the other samples, BSN5 shows a bimodal silica structure with small mesopores of around 3.4 nm in diameter and interparticle pores with sizes in the frontier of mesopores/macropores (Fig. 3). The tortuous open structure of BSN5 which form disordered and irregularly shaped intraparticle pores (Fig. 4(bI)) is also remarkable similar to that observed for the samples prepared in closed flasks (Fig. 2(b) and (c)), which suggests the negligible effect of this variable in the final properties of the silica materials, as one should expect based on their similar experimental conditions (temperature, concentrations, and pH).

XRD analysis of BSN materials shows one broad diffraction peak centred at low angles characteristic of materials with constant XRD interplanar distance but non-ordered porosity [54], independently of pH used for the synthesis of the materials. The XRD pattern of the BSN5 sample, i.e., exhibits broad diffraction peak centered at $2\theta = 1.3^{\circ}$ (see Fig. 5). The broadness of the diffraction peak is characteristic of disordered materials, as confirmed by TEM analysis. In fact, non-ordered mesopores are observed inside the network walls in the TEM micrographs obtained at high magnification, independently of pH used during their synthesis (Fig. 2 and 4(b)).

The formation of bimodal materials has been related to the competition between kinetic and thermodynamic parameters [7]. While intraparticle mesopores are due to the template effect of the surfactant micelles, the large mesopores and macropores are formed by the interparticle space between the mesoporous silica network. Therefore, the nucleation and growth mechanism, which involves the collision and aggregation of primary silica units, has a strong effect on the textural properties of the interparticle porosity [7,9,55,56].

As described in the experimental section, the surfactant used for the synthesis of BSN materials was an alkyl tetramine. To better understand the acid–base properties of this material, a tallow tetramine aqueous solution (2.5×10^{-2} mol L^{-1}, similar to that used for BSN synthesis) was titrated from pH = 2 to 12 using diluted HCl and NaOH aqueous solutions. A continuous increase of pH was observed for this pH range and thus it was not possible to determine the pK_a values of the various amines present in the surfactant. However, it was clear than as pH increased from 8 to 11 the various amines were deprotonated. So, two opposite phenomena occur as pH increases. On one hand, the surfactant becomes less cationic, on the other, the silica precursors more anionic. Therefore, it seems reasonable that for polyamine surfactants pH can be conveniently used as a simple and systematic way to control the interaction between the surfactant and the silica precursors, allowing for the suitable synthesis of hierarchical silica materials, without the need of hard templates, or the combined use of costly surfactants. One should notice that within the pH range used for this study (fairly typical for the synthesis of mesoporous silica), the interaction between the surfactant and the silica is adequate to form the so-called surfactant-templated mesoporosity, which is very similar in all the samples prepared. However, the pH control over the interaction between the surfactant and the silica precursors allows for the fine tuning of the kinetics of the silica formation and therefore the development of interparticle porosity.

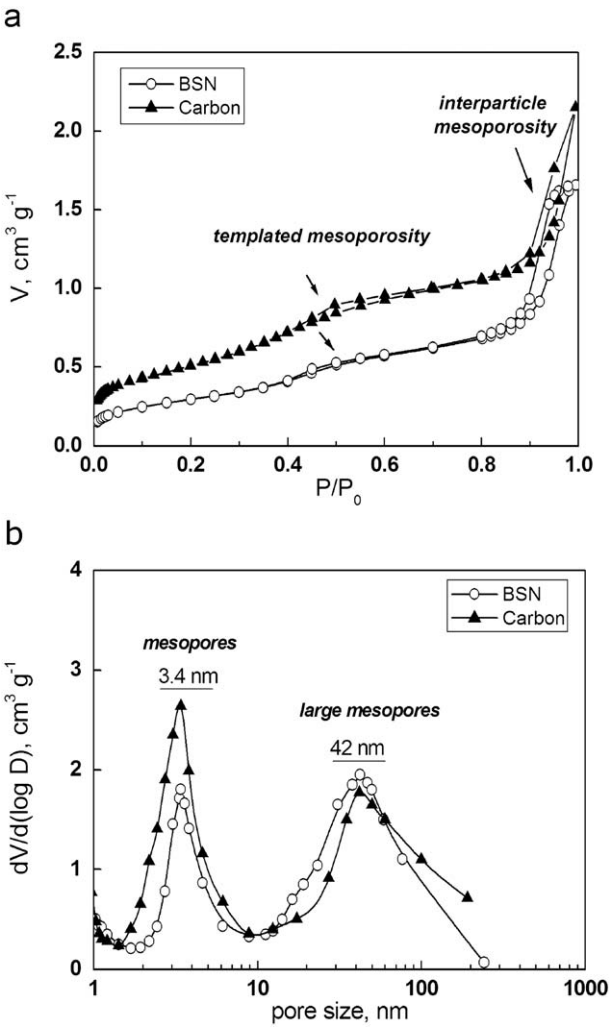

Fig. 3. Selected nitrogen adsorption/desorption isotherms at 77 K of mesoporous carbon after silica removal and its corresponding BSN5 template and (b) their corresponding pore size distributions calculated from the adsorption branch using the BJH method. The corresponding textural parameters are shown in Table 2.

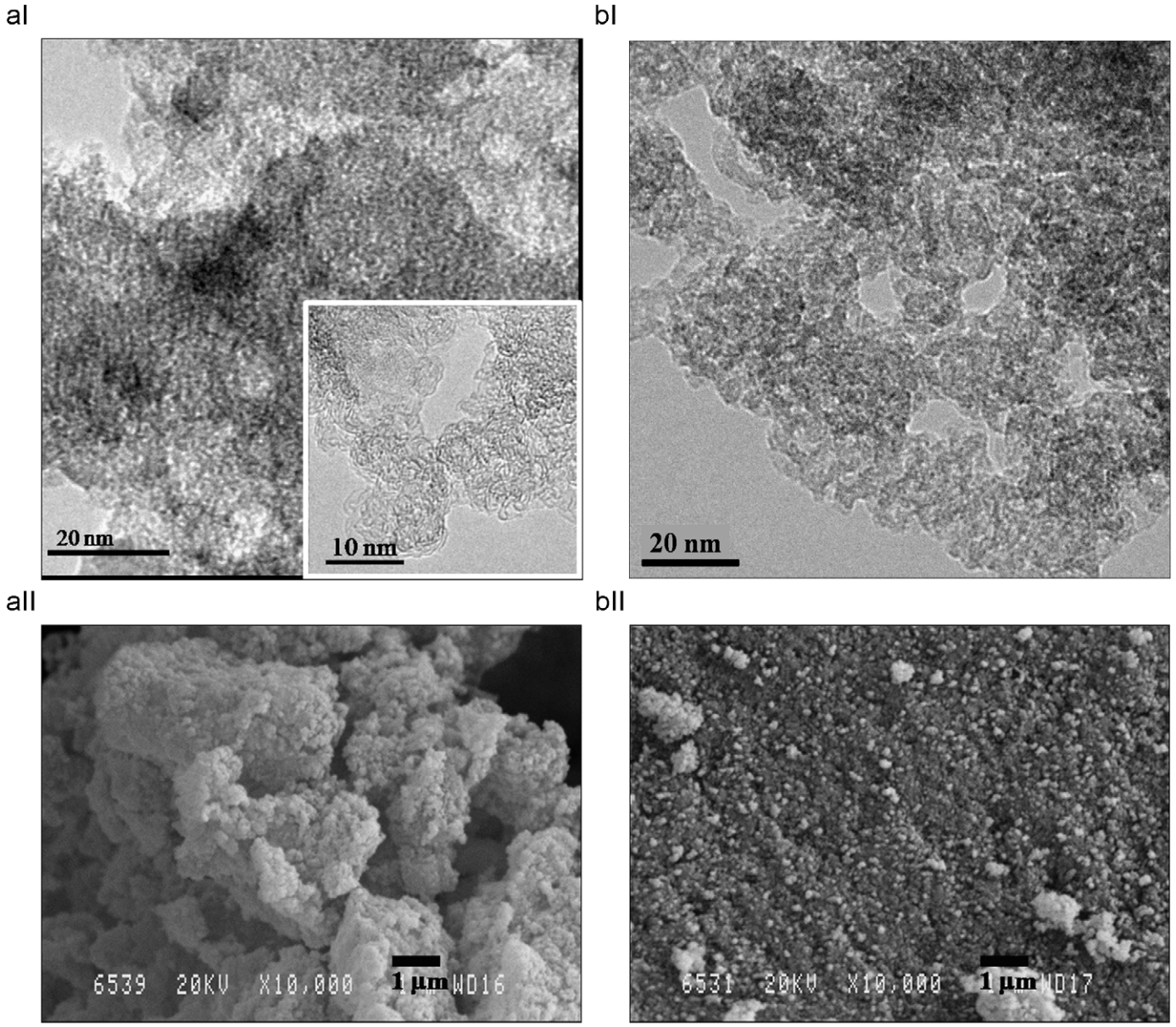

Fig. 4. TEM (I) and SEM (II) micrographs of bimodal mesoporous carbon after silica removal (a) and its corresponding BSN5 template (b). The inset in Fig. (aI) shows a TEM image of mesoporous carbon obtained a higher magnification.

Finally, the TGA curves of the BSN3 sample during and after calcination are shown in Fig. 6, with their corresponding DTG in an inset. During calcination, the BSN3 sample shows three distinctive weight losses. The first weight loss, which represents around 4 wt%, corresponds to the thermodesorption of physically adsorbed water (drying). This process nears completion at ca. 150 °C. Following, surfactant decomposition takes place between 150 and 350 °C, which accounts for a 32 wt% weight loss. Afterwards, several processes that include: residual surfactant decomposition, the combustion of the remaining organic compounds and silanol condensation take place in the third weight loss stage (in 350–540 °C range), which contributes with around 11 wt% weight loss. Moreover, by comparing TGA curves of both BSN3 before and after of calcination step (full and open symbols, respectively) it can be concluded that the calcination conditions herein employed (isothermal treatment at 550 °C) completely remove all templates from silica networks. In all cases, the TGA indicated complete removal of the tallow tetramine surfactant after calcination. Similar results have been reported for surfactant-assisted synthesis of mesoporous silica materials, i.e. MCM-41 type silica materials, where effectively, surfactant acts as template being responsible of the mesoporosity of the material [15,57,58]. Under the conditions described for these experiments, no coke deposition on the surface of any of the sample was observed; on the contrary all the silica materials were white after calcination.

The combination of templated mesoporosity and interparticle meso/macroporosity in these materials is expected to increase the accessibility of bulky molecules to the interior of these very open structures, which could have very interesting potential applications in catalysis or as hard templates.

3.2. Mesoporous carbons as replica of silica materials

As discussed in the previous section, the optimal pH to obtain bimodal silica networks with good porous properties was found to be in the 9.5–10 range. As an example, BSN5 has been used as hard

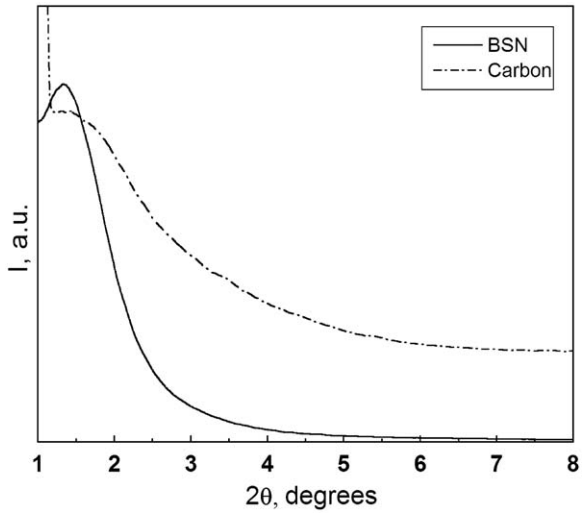

Fig. 5. Selected XRD patterns of mesoporous carbon after silica removal and its corresponding BSN5 template.

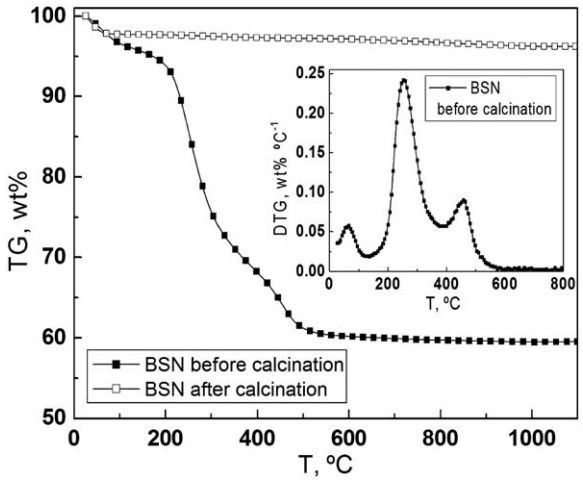

Fig. 6. Representative TGA curves for as-synthesized BSN3 before and after calcinations under nitrogen atmosphere (scan rate 10 K min^{-1}). The corresponding DTG curve before calcination step is shown in the inset.

template for the preparation of bimodal mesoporous carbon using the nanocasting technique described elsewhere to produce carbonaceous replicas of mesoporous materials [40,41,43,51].

Fig. 3(a) shows the nitrogen adsorption/desorption isotherms of both the BSN5 sample (silica template) and its corresponding carbon replica, prepared as described before and after silica removal by HF treatment (BCN). As shown in Fig. 3(a), both materials show type IV isotherms, as expected for these mesoporous materials, but the one of the BCN material shows a hysteresis loop at slightly higher relative pressures than those corresponding with its BSN5 template. The corresponding pore size distribution and textural parameters of these two materials are shown in Fig. 3(b) and Table 2, respectively. By comparing both BSN5 with its carbon replica, it is clear that both show nearly identical pore size distributions with intraparticle mesopores of around 3.4 nm and interparticle large mesopores of around 40 nm which confirms the suitability of the technique herein described to accurately replicate intricate mesoporous structures. Furthermore, the textural parameters of BCN indicates large BET areas (1190–1300 m^2 g^{-1}) and high pore volumes ($\geq$2 cm^3 g^{-1}), as evidenced by their isotherms. As observed for other carbon replicas, BCN shows a higher pore volume than the BSN template, as expected due to the lower density of carbon compared to silica and the thin carbon.

The suitability of the nanocasting process used to replicate the silica structure with carbon was confirmed by XRD analysis (Fig. 5). The XRD patterns of the carbon replica shows a broad diffraction peak centred at around $2\theta = 1.45^\circ$ that corresponds to a pore-to-pore distance of 11.6 nm, which is slightly lower than that corresponding to the silica template (12.5 nm). Thus the pore-to-pore distance of the inverse replica is only 7% smaller than that of the template. Similar results have been reported for carbon replicas obtained using sucrose or PAN as carbon sources but in that case, the carbons were highly ordered [58–60]. Both techniques, nitrogen adsorption at 77 K and X-ray diffraction confirm that the internal porous structure of the silica was properly replicated during the nanocasting process. The values obtained for the various samples prepared under identical conditions are shown in Table 2 (as a range) indicating the good reproducibility of the procedure herein described.

Fig. 4 (aI) shows a representative TEM micrograph of the BCN sample. Mesoporous carbons retain the morphology of the silica templates, as can be clearly seen by comparing both Fig. 4(aI) with (bI). It should be noted that the small mesopores of carbon replica are less discernible than those corresponding to its silica template, which is likely due to the lower electron density of carbon, producing less contrast in the TEM micrographs. The SEM micrographs of both the BSN template and the carbon replica (part II of Fig. 4) show an aggregate morphology consisting of an open and irregular structure formed by nanosized particles, being the materials highly homogeneous.

Finally, it should be noted that the carbon fraction in the carbon-silica template composite before silica template removal, determined by weight difference before and after silica removal, has been estimated to be in 25–38 wt% range, being the yield of the overall process around 18–25% (i.e. an average of 0.22 g of carbon per silica gram). The obtained results point out that bimodal mesoporous carbons with high BET areas and high pore volumes can be successfully obtained by applying the methodology herein described.

4. Conclusions

A bimodal silica material (BSN) has been prepared using an alkyl polyamine surfactant and TEOS as a silica precursor at room temperature in a one-pot synthesis. The textural properties of the silica were control by adjusting the interaction between the polyamine surfactant and the silica precursors simply by the controlling of the pH. This is a very simple cost-effective way to develop additional interparticle porosity by controlling the kinetics of the nucleation and growth of the silica. As pH increases (from 8 to 11) the polyamines get deprotonated increasing the neutral character of the surfactant whereas the silicate species get more negatively charged. On the contrary, as the pH decreases, the polyamines get protonated increasing the cationic character of the surfactant but there are less anionic silicate species. Therefore, we found that there is an optimum around pH = 10, where the interaction between the surfactant and the silicate species favours the precipitation of small interconnected silica particles that form a large interparticle pore volume, ca. 1.5 cm^3 g^{-1}. However, this interaction, within the pH range studied, is sufficient to produce the so-called surfactant-templated mesoporosity, with narrow pore size distribution, a good pore size (ca. 3.0 nm) and pore volume (0.6 cm^3 g^{-1}). The use of alkyl polyamine surfactants, which are commercially available and inexpensive, is a good

alternative to cationic surfactants, like quaternary amines, where the interaction between the surfactant and the silicate species cannot be controlled by the tuning the cationic/neutral character of the surfactant. Finally, bimodal silica materials prepared were used as a hard template for the synthesis of carbon replica by carbonization of sucrose. The carbon replica shows similar XRD pattern, gas adsorption isotherm, and morphology to the ones of the silica template, which confirms the suitability of the method proposed for the synthesis of bimodal mesoporous carbon by nanocasting.

Acknowledgement

This research has been funded by the Spanish Ministerio de Educación y Ciencia (CTQ2005–09385–C03–02). G.A acknowledges financial support from Instituto de Cultura Juan Gil-Albert. N.L.P. is grateful for financial support under the FPI program. E.S. acknowledges financial support from Spanish MICINN through the Juan de la Cierva Program (ref. JCI–2008–2165). J.G.M. is grateful for the financial support under the Ramón y Cajal Program. The authors thank Dr. Josep Subiela for the carbonization of the cured sucrose/silica composities, Dr. Cristina Almansa Carrascosa for assistance with the Transmission Electron Microscopy and the Department of Applied Physics of the University of Alicante, and especially Dr. Carlos Untiedt, for their continuous support.

References

[1] G.J.A.A. Soler-Illia, C. Sanchez, B. Lebeau, J. Patarin, Chem. Rev. 102 (2002) 4093–4138.
[2] L. Wang, K. Lin, Y. Di, D. Zhang, C. Li, Q. Yang, C. Yin, Z. Sun, D. Jiang, F.-S. Xiao, Microp. Mesop. Mater. 86 (2005) 81–88.
[3] T. Linssen, K. Cassiers, P. Cool, E.F. Vansant, Adv. Colloid Interface Sci. 103 (2003) 121–147.
[4] D. Trong On, D. Desplantier-Giscard, C. Danumah, S. Kaliaguine, Appl. Catal. A Gen. 253 (2003) 545–602.
[5] M.E. Davis, Nature 417 (2002) 813–821.
[6] J. García-Martínez, in: B. Pignataro (Ed.), Tomorrow's Chemistry Today, Wiley-VCH, Weinheim, 2007, p. 47.
[7] L. Huerta, C. Guillem, J. Latorre, A. Beltrán, R. Martínez-Máñez, M. Marcos, D. Beltrán, P. Amorós, Solid State Sci. 8 (2006) 940–951.
[8] C.T. Kresge, M.E. Leonowicz, W.J. Roth, J.C. Vartuli, J.S. Beck, Nature 359 (1992) 710–712.
[9] J.M. Morales, J. Latorre, C. Guillem, A. Beltrán-Porter, D. Beltrán-Porter, P. Amorós, Solid State Sci. 7 (2005) 415–421 and references therein.
[10] J. Yu, J.C. Yu, M.K.-P. Leung, W. Ho, B. Cheng, X. Zhao, J. Zhao, J. Catal. 217 (2003) 69–78.
[11] N. Tsubaki, Y. Zhang, S. Sun, H. Mori, Y. Yoneyama, X. Li, K. Fujimoto, Catal. Commun. 2 (2001) 311–315.
[12] B. Zhang, S.A. Davis, S. Mann, Chem. Mater. 14 (2002) 1369–1375 and references therein.
[13] Z.-Y. Yuan, B.-L. Su, J. Mater. Chem. 16 (2006) 663–677.
[14] X.Z. Wang, T. Dou, Y.Z. Xiao, Chem. Commun. (1998) 1035–1036.
[15] X. Wang, W. Li, G. Zhu, S. Qiu, D. Zhao, B. Zhong, Microp. Mesop. Mater. 71 (2004) 87–97.
[16] W. Zhang, T.R. Pauly, T.J. Pinnavaia, Chem. Mater. 9 (1997) 2491–2498.
[17] J. El Haskouri, D. Ortiz de Zárate, C. Guillem, J. Latorre, M. Caldés, A. Beltrán, D. Beltrán, A.B. Descalzo, G. Rodríguez, R. Martínez, M.D. Marcos, P. Amorós, Chem. Commun. (2002) 330–331.
[18] J. Sun, Z. Shan, T. Maschmeyer, J.A. Moulijn, M.-O. Coppens, Chem. Commun. (2001) 2670–2671.
[19] J. Sun, Z. Shan, T. Maschmeyer, M.-O. Coppens, Langmuir 19 (2003) 8395–8402.
[20] D. Kuang, T. Brezesinski, B. Smarsly, J. Am. Chem. Soc. 126 (2004) 10534–10535.
[21] S.A. Davis, M. Breulmann, K.H. Rhodes, B. Zhang, S. Mann, Chem. Mater. 13 (2001) 3218–3226.
[22] L. Tosheva, V. Valtchev, J. Sterte, Microp. Mesop. Mater. 621 (2000) 35–36.
[23] G. Gundiah, Bull. Mater. Sci. 24 (2001) 211–214.
[24] C.F. Blanford, H. Yan, R.C. Schroden, M. Al-Douas, A. Stein, Adv. Mater. 13 (2001) 401–407.
[25] T. Sen, G.J.T. Tiddy, J.L. Casci, M.W. Anderson, Chem. Mater. 16 (2004) 2044–2054.
[26] N.T. Whilton, B. Berton, L. Bronstein, H.P. Entes, M. Antonietti, Adv. Mater. 11 (1999) 1014–1018.
[27] A. Imhof, D.J. Pine, Nature 389 (1997) 948–953.
[28] B. Zhang, S.A. Davis, N.H. Mendelson, S. Mann, Chem. Commun. (2000) 781–782.
[29] Y.-J. Lee, J.S. Lee, Y.S. Park, K.B. Yoon, Adv. Mater. 13 (2001) 1259–1263.
[30] R.A. Caruso, M. Antonietti, Adv. Funct. Mater. 12 (2002) 307–312.
[31] S.A. Bagshaw, Chem. Commun. (1999) 767–768.
[32] K.H. Rhodes, S.A. Davis, F. Caruso, B. Zhang, S. Mann, Chem. Mater. 12 (2000) 2832–2834.
[33] M.W. Anderson, S.M. Holmes, N. Nanif, C.S. Cundy, Angew. Chem. Int. Ed. 39 (2000) 2707–2710.
[34] L. Tosheva, V. Valtech, J. Sterte, Microp. Mesop. Mater. 35–36 (2000) 621–629.
[35] L. Huang, Z. Wang, J. Sun, L. Miao, Q. Li, Y. Yan, D. Zhao, J. Am. Chem. Soc. 122 (2000) 3530–3531.
[36] K. Nakanishi, J. Porous Mater. 4 (1997) 67–112.
[37] S. Muto, H. Imai, Microp. Mesop. Mater. 95 (2006) 200–205.
[38] J.W. Patrick, Porosity in Carbons: Characterization and Applications, Edward Arnold, London, 1995.
[39] H. Yang, D. Zhao, J. Mater. Chem. 15 (2005) 1217–1231.
[40] R. Ryoo, S.H. Joo, S. Jun, J. Phys. Chem. B 103 (1999) 7743–7746.
[41] S. Jun, S.H. Joo, R. Ryoo, M. Kruk, M. Jaroniec, Z. Liu, T. Ohsuna, O. Terasaki, J. Am. Chem. Soc. 122 (2000) 10712–10713.
[42] K.P. GierszalM. Jaroniec, C. Liang, S. Dai, Carbon 45 (2007) 2171–2177.
[43] Z.B. Lei, Y.G. Zhang, H. Wang, Y.X. Ke, J.M. Li, F.Q. Li, J.Y. Xing, J. Mater. Chem. 11 (2001) 1975–1977.
[44] R. Ryoo, S.H. Joo, M. Kruk, M. Jaroniec, Adv. Mater. 13 (2001) 677–681.
[45] J. Lee, J. Kim, T. Hyeon, Chem. Commun. (2003) 1138–1139.
[46] A. Taguchi, J.H. Smatt, M. Linden, Adv. Mater. 15 (2003) 1209–1211.
[47] A.H. Lu, W. Schmidt, B. Spliethoff, F. Schuuth, Adv. Mater. 15 (2003) 1602–1606.
[48] J. Pang, Q. Hu, Z. Wu, J.E. Hampsey, J. He, Y. Lu, Microp. Mesop. Mater. 74 (2004) 73–78.
[49] M. Pérez-Cabero, F.R. García-García, D. Vie, I. Rodríguez-Ramos, D. Beltrán, P. Amorós, Mater. Lett. 62 (2008) 2935–2938.
[50] A.H. Lu, J.H. Smatt, S. Backlund, M. Lindén, Microp. Mesop. Mater. 72 (2004) 59–65.
[51] Z.G. Shi, Y.Q. Feng, L. Xu, S.L. Da, M. Zhang, Carbon 41 (2003) 2677–2679.
[52] Z. Lei, Y. Xiao, L. Dang, M. Lu, W. You, Microp. Mesop. Mater. 96 (2006) 127–134.
[53] F. Zhang, Y. Yan, Y. Meng, Y. Xia, B. Tu, D. Zhao, Microp. Mesop. Mater. 98 (2007) 6–15.
[54] R.K. Iler, The Chemistry of Silica. Solubility, Polymerization, Colloid and Surface Properties, and Biochemistry, Wiley, New York, 1979.
[55] C.J. Brinker, G.W. Scherer, Sol–Gel Science. The Physics and Chemistry of Sol–Gel Processing, Academic Press, New York, 1990.
[56] M. Kruk, A. Sayari, M. Jaroniec, Stud. Surf. Sci. Catal. 129 (2000) 567–576.
[57] S.A. Araujo, M. Ionashiro, V.J. Fernandes Jr., A.S. Araujo, J. Therm. Anal. Calorim. 64 (2001) 801–805.
[58] J. Fan, C. Yu, F. Gao, J. Lei, B. Tian, L. Wang, Q. Luo, B. Tu, W. Zhou, D. Zhao, Angew. Chem. Int. Ed. 42 (2003) 3146–3150.
[59] M. Kruk, B. Dufour, E.B. Celer, T. Kowalewski, M. Jaroniec, K. Matyjaszewski, J. Phys. Chem. B 109 (2005) 9216–9225.
[60] M. Kruk, M. Jaroniec, T.-W. Kim, R. Ryoo, Chem. Mater. 15 (2003) 2815–2823.